Popular Summary
Structure of the Highly Sheared Tropical Storm Chantal
During CAMEX-4

G. M. Heymsfield, J. Halverson, E. Ritchie, Joanne Simpson, J. Molinari, L. Tian

NASA's 4th Convection and Moisture Experiment (CAMEX-4) focused on Atlantic hurricanes during the 2001 hurricane season and it involved both NASA and NOAA participation. The NASA ER-2 and DC-8 aircraft were instrumented with unique remote sensing instruments to help increase the overall understanding of hurricanes. This paper is concerned about one of the storms studied, Tropical Storm Chantal, that was a weak storm which failed to intensify into a hurricane. One of the practical questions of high importance is why some tropical storms intensify into hurricanes, and others remain weak or die altogether. The magnitude of the difference between the horizontal winds at lower levels and upper altitudes in a tropical storm, i.e., the wind shear, is one important quantity that can affect the intensification of a tropical storm. Strong shear as was present during Tropical Storm Chantal's lifetime and it was detrimental to its intensification. The paper presents an analysis of unique aircraft observations collected from Chantal including an on-board radar, radiometers, dropsondes, and flight level measurements. These measurements have enabled us to examine the internal structure of the winds and thermal structure of Chantal. Most of the previous studies have involved intense hurricanes that overcame the effects of shear and this work has provided new insights into what prevents a weaker storm from intensifying. The storm had extremely intense thunderstorms and rainfall, yet its main circulation was confined to low levels of the atmosphere. Chantal's thermal structure was not configured properly for the storm to

intensify. It is most typical that hurricanes have a warm core structure where warm temperatures in upper levels of a storm's circulation help intensify surface winds and lower its central pressure. Chantal had two weaker warm layers instead of a well-defined warm core. These layers have been related to the horizontal and vertical winds and precipitation structure and have helped us learn more about why this storm didn't develop.

Structure of the Highly Sheared Tropical Storm Chantal During CAMEX-4

G. M. Heymsfield[1], J. Halverson[2], E. Ritchie[3], Joanne Simpson[1], J. Molinari[4], L. Tian[2]

[1]NASA Goddard Space Flight Center

[2]University of Maryland Baltimore Campus

[3]University of New Mexico

[4]Department of earth and Atmospheric Sciences, State University of New York at Albany

*Corresponding author address: Gerald M. Heymsfield, NASA GSFC, Code 912, Greenbelt, MD20771; (e-mail: heymsfield@agnes.gsfc.nasa.gov)

ABSTRACT

Tropical Storm Chantal during August 2001 was a storm that failed to intensify over the few days prior to making landfall on the Yucatan Peninsula. An observational study of Tropical Storm Chantal is presented using a diverse data set including remote and in situ measurements from the NASA ER-2 and DC-8 and NOAA P3 aircrafts and satellite data. The paper discusses the storm structure from the larger scale environment down to the convective scale. Large vertical shear (850-200 hPa shear magnitude range 8-15 ms^{-1}) plays a very important role in preventing Chantal from intensifying. The storm had a poorly defined vortex that only extended up to 5-6 km altitude, and an adjacent intense convective region that comprised an MCS. The entire low-level circulation center was in the clear western side of the storm, about 80 km to the west-southwest of the MCS. The MCS appears to have been primarily the result of intense convergence between large scale, low-level easterly flow and the cyclonic vortex flow. The individual cells in the MCS such as Cell 2 during the period of the observations, were extremely intense with core diameters of 10 km and peak updrafts exceeding 20 ms^{-1}. Associated with this MCS were two broad subsidence (warm) regions both of which had portions over the vortex. The first layer near 700 hPa was directly above the vortex and covered most of it. The second layer near 500 hPa was along the forward and right flanks of Cell 2 and undercut the anvil divergence region above. There was not much resemblance of these subsidence layers to typical upper level warm cores in hurricanes that are necessary to support strong surface winds and a low central pressure.

The configuration of the convective updrafts, low-level circulation, and lack of vertical coherence between the upper and low level warming regions, likely inhibited intensification of

Chantal. This configuration is consistent with modeling of vortices in sheared environments, which suggest strongest convection and rain in the downshear left quadrant of the storm, and subsidence in the upshear right quadrant. The vertical shear profile is however different from what was assumed in previous modeling in that the winds are strongest in the lowest levels and the deep tropospheric vertical shear is on the order of 10-12 ms^{-1}.

1.0 Introduction

Observational studies have generally found that large scale vertical shear is unfavorable for tropical storm formation and intensification (e.g., Gray 1968, 1979; McBride and Zehr 2003). The vertical shear that affects tropical storm intensity is the environmental shear defined as the difference between the 200 hPa and 850 hPa winds averaged over a large area centered on the storm (e.g., DeMaria 1996). All storms have some amount of shear and why certain storms intensify is a fundamental question in hurricane research. Numerical modeling studies have suggested the primary mechanism forcing wave-number one asymmetries in rainfall distributions is vertical shear (e.g., Frank and Ritchie 2001; Bender 1997; Jones 2000). Frank and Ritchie (2001) hypothesized that a large-scale shear imposed on a storm can cause high values of potential vorticity and equivalent potential temperature (θ_e) to mix outward rather than into the eye. This results in a loss of the upper tropospheric warm core in the eye and would tend to weaken the storm by increasing the central pressure. Frank and Ritchie (1999) found that in moist simulations, shear-induced vertical velocity dipoles occur through a deep portion of the troposphere such that maximum upward motions occur in the downshear left quadrant and subsidence occurs in the upshear right quadrant. In support of this secondary circulation structure, observations have shown that strong wave-number one asymmetries occur in rainfall and vertical velocity fields with the maximum rainfall occurring on the left side of the shear vector (Marks et al. 1992; Franklin et al. 1993). Based on lightning data which is associated with strong convection, Corbosiero and Molinari (2002) found a strong preference for convection downshear left in the inner core region. Vertical shears of 10 ms^{-1} in observational studies (e.g., Zehr 1992) and 10-15 ms^{-1} in modeling studies (e.g., Frank and Ritchie 2001) have resulted in adverse effects on storm intensity; the latter modeling study found that a 15 ms^{-1} shear would tear

an intense storm apart in about a day. It is clear that improvements in tropical storm intensity forecasting depend in part on how well we understand the response of tropical cyclones to environmental vertical shear.

While shear has been linked to the strength and changes in intensity of tropical storms, the role of inner core convection on storm intensification has been the subject of numerous studies. Observationally, sudden intensification has been linked to the occurrence of "convective bursts" which are intense, long-lived ensembles of deep convection topped by an anomalously cold infrared (IR) anvil cloud mass covering an area larger than the meso-γ scale (Gentry et al. 1970, Holliday and Thompson 1979, Steranka et al. 1986, Chapter 12 by Ritchie et al. in Simpson et al. 2002, etc.). The convective towers commonly referred to as "hot towers" carry high energy, high θ_E air aloft and detrain this air into the eye leading to warming of the inner core and lowering of the central pressure (Malkus and Riehl 1960). Some of these "hot towers" may be exceptionally vigorous and overshoot their equilibrium level. A recent example of hot towers in an intensifying hurricane is in the paper by Heymsfield et al. (2001) which examined the internal structure of a convective burst and its relationship to the warm core during Hurricane Bonnie's intensification, using a synthesis of high-resolution satellite, aircraft radar, and *in situ* data. An exceptionally vigorous eyewall tower within the burst penetrated to nearly 18 km and high θ_e air detrained from the burst subsided within Bonnie's eye, and it was speculated that this might provide favorable warming for storm intensification.

Modeling studies have shown that the dynamic response to intense bursts of convection and mesoscale convective systems in the inner core of tropical cyclones is the development of discrete vortices that then mix into the vorticity core of the tropical cyclone, resulting in intensification (e.g., Ritchie and Holland 1997; Montgomery and Enagonio 1998; Ritchie 2003).

Such processes were concluded to be occurring in the genesis and eye formation processes in Tropical Cyclone Oliver (1993) (Simpson et al. 1997) and Floyd (1999) (Ritchie et al. 2002).

One of the observational difficulties in examining the vortex response to shear and the role of convection in hurricane intensification is that it requires detailed knowledge of multiple scales ranging from the larger scale storm environment, the vortex scale, down to individual convective elements. During the 2001 Atlantic hurricane season, NASA and NOAA conducted an extensive field campaign to study hurricanes on multiple scales and covering multiple objectives (Hood et al. 2004). NASA's component, the Convection and Moisture Experiment 4 (CAMEX-4), combined with an enhancement of NOAA's Hurricane Field Program (HFP2001), resulted in an unprecedented study of hurricanes from the upper levels of the atmosphere (NASA) through the middle levels of the atmosphere (NOAA) to the boundary layer (NASA).

In light of the previous observations on the role of vertical shear and convective bursts on storm intensification, we examine Tropical Storm Chantal during CAMEX-4, which had very intense convection but failed to intensify in moderate to strong environmental shear. On 20 August 2001, the NASA high-altitude (20 km) ER-2 and medium-altitude (9-12 km) DC-8 aircraft, and the lower-altitude (3-6 km) NOAA P3 (NOAA-42), conducted a coordinated Quantitative Precipitation Estimation (QPE) mission focused on a strong region of convection close to Tropical Storm Chantal's low-level center of circulation (Black et al. 2001). The NASA (ER-2 and DC-8) and NOAA (P-3) aircraft based at Jacksonville and Tampa, Florida, respectively, flew east of the Yucatan-Belize coast for this mission. An intense convective burst episode was occurring during the aircraft flights, and the ER-2 and DC-8 were stacked close in time and location, with the ER-2 over the top of the burst and the DC-8 penetrating it. The NASA aircraft collected remote sensing (radar, radiometer), *in situ*, and dropsonde data sets,

while the P3 collected radar, *in situ*, and dropsonde data at lower levels. The ER-2 and DC-8 were each instrumented with downlooking radars called ER-2 Doppler radar (*EDOP*, Heymsfield et al. 1996) and the DC-8 Precipitation Radar-2 (*PR-2*, Sadowy et al. 2003) as well as various other instruments described elsewhere in this journal issue. EDOP, a focus in this paper, is a fixed dual-beam X-Band radar (nadir and forward-looking beams) from which vertical and along-track horizontal winds can be calculated (Heymsfield et al. 1996).

There are several objectives of this paper. These are: 1) To analyze the mesoscale structure of a non-developing tropical storm from the surface through various upper levels to illustrate the relationship of Chantal's intense convection (a convective burst) to the low-level vortex, winds, and moisture, the tropospheric warm anomaly, and the tropospheric shear using a synthesis of P3 and DC-8 flight-level data, dropsondes, and satellite (GOES and TRMM Microwave Imager (TMI)) information. This will help in understanding why the intense burst was sustained to the east-northeast of the vortex for such a long time. And, 2) To use the analyzed fields in (1) above as a mesoscale context, to examine the convective-scale features of the burst i.e. updraft/downdraft structure, reflectivities, and θ_e using the high resolution two-dimensional ER-2 Doppler Radar (EDOP) measurements. The ER-2 Doppler vertical motions inside the burst will be corroborated with the in situ DC-8 penetration data. Our hypothesis is that the low level and mid level warm anomalies are decoupled due to strong environmental shear. This will help understand the role of vertical shear on decoupling the storm's convection from Chantal's low level vortex and the relation between the convective scale structure and the mesoscale environment.

2.0 Large-scale storm environment and convective burst evolution.

Chantal first became a depression on 14 August, a weak tropical storm on 17 August, and it weakened slightly early on 20 August and re-intensified later in the day just prior to landfall. The storm was forecast to intensify early on 20 August and eventually made landfall near the Yucatan-Belize border early on the 21st August (Fig. 1). The minimum sea level pressures (MSLP) ranged from 1008 hPa on 19 August to a minimum of1001 hPa late on 20 August (Fig. 1, Fig. 2, Panel A). The maximum surface winds (MSW) increased from ~25 ms^{-1} to 30 ms^{-1} early 19 August, and then fluctuated from 28-30 ms^{-1} until landfall early on 21 August (Fig. 2, Panel A). Chantal's movement was west-northwest (255-285°) from 18-20 August, and its speed continually decreased from a peak of 12 ms^{-1} late on 18 August, to about 4 ms^{-1} near landfall (Fig. 2, Panel B).

Since the environment soundings were very sparse in Chantal's environment, the 200-850 hPa vertical shear during this period was calculated based on the National Centers for Environmental Prediction (NCEP) final analyses, which are 1° global analyses based on the Global Forecast System (GFS formerly AVN) but with a synoptic time +6 hour cutoff so more data makes it into the analysis. The horizontal winds were averaged at the 850 and 200 hPa levels over a 600 km radius centered on the National Hurricane Center's (NHC) best track position and shear was calculated from the difference between the winds at the two levels (Fig. 2, Panel C). The plot shows a distinct shear minima (<5 ms^{-1}) on 18 August/1200 UTC, and Chantal appears to intensify to its lowest central pressure (994 hPa) during the subsequent 18-24 h. During this intensification period, the shear magnitude increased and became strong (> 10 ms^{-1}) from 19 August/0000 UTC until about 20 August/1200 UTC. The shear peaked (>15 ms^{-1}) at 0600 UTC on 19 August near the time when Chantal achieved its lowest central pressure, and after this peak the shear decreased with local minima at 20 August/1800 UTC and 21

August/1800 UTC. Given that Chantal appeared to be intensifying through this period, the high shear magnitudes are very surprising but it suggests the storm takes time to respond to shear, which has been modeled by Frank and Ritchie (2001) and observed by Gallina and Velden (2002). The shear direction is generally 260-270° from 19 August/1200 UTC to 20 August/1200 UTC, and then backs 45° over the next 36 h.

The general precipitation structure associated with Chantal is depicted in Fig. 3 with the GOES visible and 10.8 μm IR image at 2002 UTC on the 20th of August, and the TRMM Microwave Imager (TMI) 85 GHz temperatures at 2034 UTC. The approximate location of Chantal's low-level center of circulation is shown west-southwest of an intense convection region which produced cold IR (~193K) and 85 GHz temperatures (~126 K) (Figs. 3B and 3C, respectively). This region is representative both in location relative to the circulation center, and intensity of the convective activity associated with Chantal on 19-20 August.

Since Chantal was located far from the NASA and NOAA aircraft bases and the NASA aircraft were not authorized to fly over Mexico, it was decided to focus on the heavy rain region over water in the right rear quadrant of Chantal. Flight planning by NOAA and NASA scientists allowed for excellent coordination between the aircraft. On several passes, the ER-2, DC-8, and P3 when possible due to its lower airspeed, were stacked vertically. The DC-8 and ER-2 performed three main passes across the storm (labeled 1-3 in Fig. 3B). The DC-8 experienced severe icing during the first flight leg which required a descent to lower altitudes from its nominal 12 km altitude and a diversion around Cell 2 during Pass 2. After Passes 1-3, the aircraft then focused on the heavy convective rainband further northeast of the core of Cell 2. The P3 performed shorter passes, sometimes coordinated with the ER-2 and DC-8 (Fig. 3C), at other times focused on flight legs for Doppler analysis.

The general state of the surface conditions, which Chantal encountered during 19-20 August was obtained from TRMM-TMI derived SST (Fig. 4A), and the QuikSCAT derived surface winds (Fig. 4B). The GOES IR contours at 200 K and 240 K at 0000 UTC on 20 August near the time of the QuikSCAT data, are shown on the figures for position reference. The microwave-based SST's (Wentz et al. 2000) from the standard 3-day average from 18-20 August 2001 show the storm moved into warmer (30°C) water on 20 August. The SST's southeast of the storm were cooler (~29°C). The surface winds obtained from the JPL Level 2B wind product (QuikSCAT 2001), were strong easterlies with a large curvature north of the Chantal's precipitation region, and weak easterlies to the south of the storm track. Strong mesoscale confluence is noted on the east-northeast portion of the storm, which provides forcing for the convection as will discussed later in Section 4. There is not a well defined circulation in the winds because the storm motion is ~ 6 m s^{-1} to the west, which is strong enough to mask any low-level circulation.

The synoptic scale vertical structure associated with Chantal is best depicted through a combination of conventional soundings and forecast model winds. Figure 5A-C show 1200 UTC soundings from west to east across the region shown in Fig. 1 (Merida, Mexico (MID), Grand Cayman (KCR), and Kingston, Jamaica (KJP)). These soundings were north of the storm track and there were no soundings south of the storm track on 20 August. The storm environment horizontal winds and vertical wind shear vector derived from the 20 August/1200 UTC NCEP final analysis is shown in Fig. 5D. The soundings show strong large scale, zonal-reversing flow with low-level easterly flow 10-20 m s^{-1} up to about 6 km altitude, and southwesterly flow 10-20 m s^{-1} in the upper troposphere (> 9 km altitude). The averaged model-derived storm environment winds have lower magnitudes with ~8 m s^{-1} low-level easterly flow and 4 m s^{-1} westerly flow near

200 hPa. Part of this model-observation difference is the inability of the NCEP final analysis to capture mesoscale details of the storm and part is the effects of averaging which will tend to reduce observed peak values. Also, the observed winds are stronger on the north side of Chantal and there were few soundings on the south side of the storm where weaker values would be located. Chantal's motion is mostly toward the west (~ 6 m s^{-1}) so the storm-relative winds are very weak.

Figure 6 shows a sequence of color enhanced GOES cloud top temperatures covering the aircraft flights 2002-2332 UTC on 20 August. A strong convective burst that consists of several large cells occurs during this image sequence. Cell 2 is centered in the first image at 2002 UTC and another strong cell (Cell 3) develops about 3 h later at 2302 UTC. Cell 2 rapidly develops both in lower cloud top temperatures and expanding anvil (dashed lines) over a two-hour period. Convective activity 12-18 h prior to this burst was sporadic with occasional strong cells but none which produced rapid anvil expansion as shown in Fig. 6. In general though, smaller bursts were continually redeveloping in at least two main regions, often separated by 100-200 km and located to the east-northeast of the low-level circulation center. These intense bursts evolved in the IR imagery from cold, overshooting tops, to expanding anvils, to dissipation, over a few hours. The rapid expansion of the temperature contours relative to the much smaller expansion of the overshooting top area in Fig. 6 imply strong upward mass fluxes produced by cells during this period. The cells moved to the west with the storm rather than being formed by a relatively fixed area of overshooting hot towers. The contribution of individual cells to forming a larger scale burst is similar to the succession of cells that formed in Hurricane Bonnie's convective burst (Heymsfield et al. 2001). The environmental shear vector shows (Fig. 6, 2002 UTC panel)

that Cell 2 located downshear to downshear left as suggested in both the observational and modeling studies mentioned in the Introduction.

The rapid growth of this burst is shown quantitatively in Fig. 7 with the minimum (cloud top) temperature of Cells 1-3 (Panel A) and anvil area expansion associated with Cells 2 and 3 (Panel B). The area curves were constructed from the sequence of ~15 min GOES IR images on 20 August by obtaining the number of pixels with IR brightness temperatures less than 194K, 196K, and 198K centered on the convective burst. It was not possible to track higher temperature contours since they merged together from different cells. This burst in Fig. 7 was by far the strongest during 20 August. Rapid growth of Cell 2 to over 4000 km^2 is evident between about 2000 and 2130 UTC, and then its area declines from 2130 to 2230 UTC. The IR temperatures associated with this cell reach a minimum of ~193K at about 2110 UTC, 20 min prior to the area maximum; a new cell begins development at ~2300 UTC[1]. The approximate stages of development of Cell 2 are shown on the figure: the growth period which occurs before and during the anvil expansion prior to the minimum temperature occurrence; mature convection during the anvil expansion; and weakening stage during which the anvil area decreases and the cloud top temperatures increase. Also indicated on the figure are times when the NASA aircraft crossed Cell 2 during three flight legs; the DC-8 circumnavigated Cell 2 during Pass 2 due to prior icing conditions during Pass 1. Pass 1 and 2 occurred during the active development of Cell 2, and Pass 2 occurred during the dissipation of the burst. The P3 focused on this cell and later on Cell 3, which was not studied by the NASA aircraft.

[1] The TRMM VIRS temperatures were lower than the GOES IR values probably because of the better VIRS resolution as compared with GOES (1 km pixel size versus 4 km) and the small dimensions of undiluted portions of individual cells.

3.0 Mesoscale storm environment from dropsondes and flight level data.

a. Thermodynamic and wind analyses.

The mesoscale environment of Chantal is examined here using a combination of dropsonde and DC-8 and P3 flight level data. The DC-8 and P3 dropped 7 and 23 dropsondes, respectively, mostly near the circulation center and on the eastern side of the storm (Fig. 8); only a few of the dropsondes were located on the west side of the circulation. Details on the dropsondes are described in Hock and Franklin (1999). The P3 flew between 4.2 to 4.4 km altitude with a mean of 4.3 km, whereas the DC-8 flew over a wider altitude range between ~10.5 to 12.6 km most of the time with a mean ~11.7 km, but with one flight leg (Pass 2) at ~9 km altitude. From these data sets, two-dimensional maps of various thermodynamic and winds were constructed at the mean aircraft altitudes of 11.7 km and 4.3 km (Figs. 9A and 9B, respectively), and near the surface at 0.2 km (Fig. 9C) using only the dropsondes. The DC-8 flight level data used wind data from the Meteorological Measurement System (MMS) [Bui 1997] and moisture data from the JPL Laser Hygrometer (JLH) [May 1998]. Figures 9A and 9B provide storm-relative wind barbs (storm motion of 6 m s^{-1} toward 290°), θ_e contours, streamlines and background images of GOES IR at 2115 UTC (Fig. 9A), TMI 85 GHz (Fig. 9B), and TRMM 10 GHz (Fig. 9C). The locations of both the aircraft flight level and dropsonde data have been space-time adjusted to 2115 UTC since the data sets cover 3 hours and the storm has moved ~65 km during this time. Narrowing the range of DC-8 altitudes has reduced the variation of θ_e from changes in the aircraft altitude. It is noted here that in some cases there may be an offset between the satellite and aircraft observations due to mapping errors in the satellite data arising from parallax or navigation errors. This can be on the order of 10-20 km for either satellite.

At 11.7 km DC-8 level (Fig. 9A), the large-scale southwest flow strongly diverts around Chantal's convective region. Strong outflow divergence is produced by Cell 2 that extends nearly 100 km upshear. The high θ_e (352 K) contour covers most of the convective region and it also covers the outflow divergence in the winds; a 354 K θ_e region exists upshear of the precipitation core of Cell 2. Thus it appears that the 352-354 K θ_e is representative of the convective core.

At the 4.3 km altitude (Fig. 9B), a well-defined circulation center is observed that is tilted slightly northeast of the low level circulation (LLC) position at 0.2 km. A northwest-southeast band of high 350-352 K θ_e (peak value 354-355 K) is located about 20-30 km southwest of the intense 85 GHz precipitation core of Cell 2. This displacement between the high θ_e band and the core of Cell 2 is due to the northeast tilt of the system that will be discussed further in Section 4.

The LLC center is located ~80 km southwest of the main cell (Cell 2 in Fig. 9C). High θ_e air (363 K) feeds the convection from the south side and converges spirally into an inflow notch northeast of the LLC. To the northeast of the convection, there is a broad pool of rain-cooled air with θ_e values 335 K or less. This is the cumulative effect of cold downdrafts in the stratiform precipitation to the east. There was a large θ_e gradient north-south between the inflow sector and the outflow boundary along the southern side of Cell 2. Strong easterly flow was present north of the LLC in the rain-cooled air. The pressure distribution (not shown) shows that the lowest pressure (982 hPa) was not associated with the LLC but rather with a mesolow across the main outflow boundary and θ_e ridge (350 K) northeast of the LLC ("L" in Fig. 9C). The surface flow is highly confluent into this mesolow with a 25 m s^{-1} easterly low level jet (green contour) at the surface, which is probably being accelerated into this mesolow. The inflow notch, not the LLC, has the greatest flow confluence, highest wind speeds, lowest surface pressure and highest θ_e.

This is all feeding the massive Cell 2 hot tower that will be discussed further in Section 4. The inflow notch region and Cell 2 seems to be dynamically the most active region and not the LLC. There still may be lower pressures associated with the LLC, but the west side of the LLC was not sampled well by aircraft or dropsondes.

Figure 10 shows profiles from dropsondes released by the DC-8 (2131, 2125, 2036, and 2101 UTC) at locations shown in Fig. 9C that capture key features of Chantal's structure. The Convective Available Potential Energy (CAPE) was calculated for these soundings using average temperatures over the lowest 500 m to avoid large CAPE values near the surface. The CAPE for a particular sounding was chosen as the largest value between the boundary layer and 700 hPa, so that erroneously large near surface values from shallow cumulus downdrafts, etc., are avoided. The soundings show the general stability structure in Chantal: suppressed CAPE upshear (1077 Jkg^{-1} at 2131 UTC, Fig. 10A), nearly 500 Jkg^{-1} more of CAPE downshear and downshear left (1554 Jkg^{-1} at 1554 UTC in Fig. 10B, 1524 Jkg^{-1} at 2036 UTC in Fig. 10C), and zero CAPE in the stratiform region to the east (2101 UTC, Fig. 10D). The use of CAPE in this context is reasonable since upright rather than slantwise convection is dominant in Chantal.

b. Warm core structure and mid-level subsidence

The data is examined here for the presence of a warm anomaly at lower and middle levels in the P3 and DC8 dropsonde data. How big is this anomaly, and where is it located with respect to both the MCS and the low level vortex? Figure 11 (Panels A-D) provides plots of the temperature perturbations (T') at the surface (50 m), 3 km, 6 km, and 8 km altitude over the same domain as in Fig. 9. The pressure perturbation (P') at the surface and 3 km levels is also shown in Figs. 11E, F. These perturbations were obtained by subtracting the temperature-height

or pressure-height profile representative of the storm environment. These profiles were constructed by averaging soundings and dropsondes that were further out from Chantal's LLC (i.e., Fig. 5 and more distant DC-8 sondes).. An unsuccessful attempt was made to incorporate the flight level data into the temperature analysis due to the varying height of the aircraft and the inability to correct the temperatures for these height changes. Since the dropsondes have incomplete coverage of the plot domain, we have contoured only a limited region.

The near surface level T' (SFC, Fig. 11A) depicts a weak warm region east-southeast of the LLC with a peak value of +1.3 C and slightly larger maximum of +1.9 C at the 2 km level (not shown). Two low-pressure areas exist, one near the LLC (-5.7 hPa) and the other stronger area (-6.3 hPa) at the edge of Cell 2. This latter meso-low is an inflow notch for Cell 2 and the generally reflects the high θ_e air entering the MCS. An extensive area of low T' with a minimum of –2.5 C exists below Cell 2 which is associated with the rain-cooled air previously mentioned. At 3 km (Fig. 11B), there is significant warming over the LLC with a local maxima of T'=+4.6 C. This largely results from subsidence warming observed in the 2131 UTC sounding (Fig. 10A) which is also in the upshear right quadrant. The two low pressure areas still exist but with greatly reduced magnitude over the LLC (-P'~2.8 hPa), and still a strong pressure minimum (P'~-4.6) immediately adjacent to Cell 2 and at the head of its inflow. At 6 km (Fig. 11C), the warm core (maximum value +1.9 C) has shifted from the LLC, east-northeastward along the shear vector. Part of this warming occurs along the upshear right periphery of Cell 2 and partially within the cell itself. At the 8 km altitude (Fig. 11D), an expanded warm region (T' maxima of ~1.5 C) occurs along the upshear and upshear right periphery of Cell 2. And, by 10 km (not shown), there is no warm core outside of the Cell 2 cloud region.

Summarizing the above temperature structure, Chantal does not have one deep warm core but rather two areas of anomalous, weak warming. One area is in the clear air directly above the LLC and seems most pronounced in the lower levels (<6 km altitude). The 2131 UTC and 2125 UTC dropsondes (Figs. 10a,b) corroborate this warming and suggest intense subsidence warming (i.e., an inversion) in the 600-800 hPa layer. A second warm area above 5 km is more diffuse but is consistently located over the inflow notch (high θ_e inflow in Fig. 9C) in the vicinity of the most intense hot tower (Cell 2), and has vertical continuity from about 4-5 km to 8 km. The warming in the lower layers that is localized to the inflow notch/updraft area, is possibly due to enhanced surface heat fluxes and lack of convective downdrafts. The warming in the upper layers is more spread out and on the edge of the MCS, and there are several possible mechanisms for this broad area of mid-level warming: 1) from compensating mid-level subsidence, 2) induced by the mesolow inside Cell 2 and/or latent heating in the cell, and 3) the easterly outflow aloft colliding with the upper-level environmental westerlies causing subsident warming (e.g. Ritchie and Elsberry 2001). Further discussion on this will be given in the next section. It is apparent that the weak, shallow warm core in Chantal is unfavorable for lowering the storms central pressure.

4.0 Convection and sustenance mechanisms

The convective region in Chantal was vigorous and long-lived and one key question is what maintains this convection and how does it interact with the shallow vortex described in the previous section. Another key question is whether the low-level observed warming adjacent to Cell 2 and upshear right of the LLC is due to convective-induced subsidence or shear-induced subsidence (Ritchie and Elsberry 2001). The EDOP data from ER-2 passes across the

convection and LLC, provide some insights on the above questions. The main three ER-2 and DC-8 passes across Chantal covered ~2010-2030 UTC (Pass 1), ~2101-2125 UTC (Pass 2), and ~2148-2224 UTC (Pass 3) as shown in Fig. 3B. EDOP was not turned on until near the end of Pass 1, so cross sections from Passes 2 and 3 are presented in the following. Figure 12 shows the EDOP-derived cross-section for Pass 2, and Fig. 13 for Pass 3. The analysis procedures for the EDOP data are discussed in Heymsfield et al. (1999, 2001) and the procedures here are similar. The reflectivity image is shown in Figs. 12A and 13A along with storm-relative wind vectors in the cross-section and contours of θ_e. Figures 12B and 13B show an image of the along-track storm-relative wind component (u_r) derived from EDOP dual-beam data, superimposed contours of tangential wind (v_r), and streamlines of airflow. The vertical profiles in the reflectivity images are attenuation corrected using the surface reference approach, and vertical air motions in the wind vectors are estimated from the Doppler velocities using hydrometeor fallspeeds based on empirical relations in the above papers. The largest uncertainties occur in convective regions where there is mixed phase occurring above the freezing level. The wind vectors in the plane of the cross-section have been obtained from EDOP's dual-beams, and are presented as storm-relative assuming a storm motion 6 ms^{-1} toward 290°. The θ_e values in Figs. 12 and 13 were derived from both the DC-8 and P3 dropsonde and flight level data mapped to the cross-section; these did not cover the entire cross-section so some of the contours terminate or have arrows to denote this.

a Pass 2: Along-shear vertical structure (Fig. 12)

There are several prominent features evident in this section which is approximately along the shear vector: 1) The LLC depicted by the v_R contours in Panel B, is located at a distance of

~30 km in the figure. 2) The major Cell 2 in Pass 2 in panel A (distance scale ~110 km) is extremely intense with peak reflectivites exceeding 55 dBZ, cloud top extending up to 17 km altitude, which is well above the tropopause. The earlier DC-8 flight through this convection (Pass 1) recorded 22 ms^{-1} peak updrafts, ~10 km wide region of updrafts greater than 5 ms^{-1}, and peak θ_e of 355-356 K in the convection core. The DC-8 flight level data during Pass 2 did not pass through Cell 2's core, but still recorded 8 ms^{-1} updrafts and θ_e of ~356 K; the environment θ_e was ~350K. 3) This strong cell produces larger upper-level diffluence above 11 km altitude, and the high θ_e air carried aloft from low levels diverges over 200 km from the updraft core, producing a warm core above the convection and not above the LLC. 4) A large rain-cooled region is located at low-levels with θ_e ~330-340K below a pronounced bright band that is produced by the stratiform precipitation on the east side of the convection. The low-level easterlies particularly below 1 km altitude that are faster than Chantal's motion east of the storm, pass through this rain-cooled region and confluence results along the leading edge of this rain-cooled air with an inflow jet feeding Cell 2. This inflow jet of high-speed, high θ_e air feeding Cell 2 is located at distance 110 km, low-levels in Fig. 12B. 5) Upper-level (5-10 km altitude) westerly flow subsides on the west side of Cell 2 above the LLC, and undercuts the upper-tropospheric outflow from the cell. The interaction of the westerly shear with this strongly divergent outflow likely results in a broad subsidence warming region near the cell (Figs. 11C and 11D). 6) The vortex center tilt based on the flight level data at the DC-8 and P3 altitudes, is highly sheared to the east.

b. Pass 3: Convection tilt (Fig. 13)

Pass 3 is located east of the LLC, running southwest to northeast (Fig. 3B), and it emphasizes the tilt of Cell 2 as it was weakening. There are several additional features to note from this pass. 1) The updraft has a strong north-northeast tilt over the rain-cooled easterly flow and it has a top of about 16 km. 2) There is strong horizontal shear between the high θ_e air to the south (i.e., inflow) and the low θ_e air in the rain-cooled air to the north-northeast. The rain-cooled air is located below about 4 km altitude. 3) The DC-8 measured an updraft ~8 ms^{-1} at 2205 UTC (distance ~230 km in figure) with a spike of θ_e ~358 K, but with more typical 354 K values in the updraft core. Again, this high θ_e could only originate in the inflow sector air, south of the convection. 4) High θ_e air (353-355 K) again exists in the upper-level divergent outflow region near 12 km altitude. The DC-8 *insitu* winds have strongly divergent winds at 12 km altitude near the Cell 2 core (Fig. 9A). 5) There are mid-level downdrafts along the southwest flank of the cell (distance ~160-190 km and altitude 8-10 km) which are related to the gentle subsidence mentioned in Section 4.a.

5.0 Summary and conclusions.

The Tropical Storm Chantal study presented here has provided one of the first observational studies examining a weak tropical storm that struggled to intensify in a highly sheared environment. Figure 14 summarizes Chantal's three-dimensional structure as deduced from the observations. The unusual aspect of Chantal was that it had a poorly defined vortex that only extended up to midlevels, and an adjacent intense convective region that comprised an MCS. The LLC center was in the clear region about 80 km to the west-southwest of the MCS, a configuration that may have inhibited intensification of the storm. The MCS appears to have

been primarily the result of intense convergence between large scale, low-level easterly flow and the cyclonic vortex flow. The individual cells in the MCS such as Cell 2 during the period of the observations, were extremely intense with core diameters of 10 km and peak updrafts exceeding 20 m s^{-1}. The easterly flow supporting the convergence was rain-cooled resulting in a strong thermal boundary with the high-θ_E air feeding the strongest Cell 2. It is unclear whether this strong low-level thermal gradient resulted in vertical vorticity generation baroclinically across the gradient and then tilted into the vertical. Associated with this MCS were two broad subsidence (warm) regions both of which had portions over the vortex. The first layer near 700 hPa was directly above the vortex and covered most of it. The second layer near 500 hPa was along the south and southwest flanks of Cell 2 and undercut the anvil divergence region above. There was not much resemblance of these subsidence layers to typical warm cores in hurricanes. The clear air over a large portion of Chantal's LLC suggest that convection is being suppressed by shear-induced downdrafts in the free atmosphere in the clear air.

There are strong parallels between the mesoscale structure of Chantal as compared with the genesis of Tropical Cyclone Oliver (1993) although Oliver had much weaker shear (Simpson et al., 1997). In the Oliver study, there were multiple regions of warming. Some warming occurred in the clear air outside the main MCS region that was attributed to subsidence near where the eye was starting to form in that storm. It is obvious that the mechanisms for mid- and upper-tropospheric warming require further study due to the many possible configurations of MCS's relative to the storm's circulation.

The observed structure of Chantal relates in a general sense to theoretical and modeling studies of a vortex in a sheared environment. The convection in Chantal forms downshear left, and the free-atmosphere subsidence in the clear air at low levels with associated warming was

found to be upshear as we would expect from the Ritchie and Elsberry (2001) moist results. The observed large vertical shear toward the northeast in Chantal resulted in a strong upper-level relative flow toward the northeast. This shear had a significant effect on the storm intensification in that it mechanically tilted the burst away from the LLC. Most of the observed warming at upper levels was produced by the strong convective cell (Cell 2) and was carried off to the northeast by the strong relative flow, rather than over the LLC as typically observed in strengthening systems where deep warm cores help lower central pressures. Frank and Ritchie (2001) mention that asymmetries occur in the upper troposphere where high values of θ_E and potential vorticity are mixed outward rather than into the eye. They speculated that shear ventilates the eye resulting in a loss of the warm core at upper levels, which raises the central pressure and weakens the storm.

The observations presented here represent one case where shear has an important role in preventing a storm from intensifying. The original objectives for the Chantal mission were not to study the role of shear on the storm but rather the structure of the convection. As a result, there were barely enough dropsondes on the west side of the LLC for this study. It is clear that shear and other factors are key in understanding why some storms intensify and others don't. These require a combination of focused observational studies, which provide more complete information of the storm details, and a broader set of assumptions in the modeling that incorporates more of the observational results. For example, the shear profile in Chantal is different from that assumed in many modeling studies. In Chantal, the strongest winds are in the lowest levels of the atmosphere, i.e., "bottom up" shear. Most of the idealized runs have been "top down" shear.

Acknowledgements

The primary authors work was supported under the NASA CAMEX-4 research announcement sponsored by NASA Headquarters program manager Dr. Ramesh Kakar. We are especially appreciative of Drs. Michael Black and Frank Marks of the Hurricane Research Division of NOAA who were a critical part of obtaining the data sets from Chantal and for providing basic information and mission summaries. We have had scientific discussions with Dr. John Gamache and others at HRD. On the NASA side, Ms. Robbie Hood and Dr. Ed Zipser were key in directing the mission on this day and many others provided key roles in the Chantal flights. Numerous data sources were used for this paper for which we are grateful. A number of the data sets were obtained from the CAMEX-4 archive at the Global Hydrology Resource Center sponsored by NASA's Atmospheric and Remote Sensing Program. Mr. Paul Bui of Ames Research Center (MMS instrument) and Dr. Robert Herman of JPL (JLH instrument) are especially acknowledged for providing DC-8 flight level winds and moisture, respectively.

References

Bender, M. A., 1997: The effect of relative flow on the asymmetric structure of the interior of hurricanes. *J. Atmos. Sci.*, **54**, 703-724.

Black, M.L., J. Gamache, P. Dodge, G. Barnes, F. Marks, J. Hudson, and T. Castells, 2001: Mission summary: Tropical Storm Chantal. NOAA, Hurricane Research Division, 23 pp. [Available from NOAA, AOML, Hurricane Research Division, 4301 Rickenbacher Drive, Miami, FL 33149-1026]

Bui, T. P., 1997: DC-8 Meteorological Measurement System. SONEX Workshop, NASA Ames Research Center. [Available from NASA Ames Research Center, M.S. 245-5, Moffett Field, CA 94035-1000]

Corbosiero, K. L., and J. Molinari, 2002: The Effects of Vertical Wind Shear on the Distribution of Convection in Tropical Cyclones. *Mon. Wea. Rev.*, **130**, 2110–2123.

DeMaria, M., 1996: The effect of vertical shear on tropical cyclone intensity change. *J. Atmos. Sci.*, **53**, 2076-2087.

Franklin, J. L., S.J. Lord, S.E. Feuer, and F.D. Marks, 1993: The kinematic structure of Hurricane Gloria (1985) determined by nested analyses of Dropwindsonde and Doppler radar data. *Mon. Wea., Rev.*, **121**. 2433-2451.

Frank, W. M., and E. A Ritchie,. 2001: Effects of Vertical Wind Shear on the Intensity and Structure of Numerically Simulated Hurricanes. *Monthly Weather Review*: Vol. 129, No. 9, pp. 2249–2269.

_____, and E. A. Ritchie, 1999: Effects of Environmental Flow upon Tropical Cyclone Structure. *Monthly Weather Review*: Vol. 127, No. 9, pp. 2044–2061.

Galina, G. M., and C. S. Veldon, 2000. A quantitative look at the relationship between environmental vertidcal wind shear and tropical cyclone intensity change utilizing enhanced satellite derived wind information. *Preprints, 24th Conf. on Hurricanes and Tropical Meteorology*, Ft. Lauderdale, FL, Amer. Meteor. Soc., 256-257.

Gentry, R.C., T.T. Fujita and R.C. Sheets, 1970: Aircraft, spacecraft, satellite and radar observations of Hurricane Gladys, 1968. *J. Appl. Meteor.*, **9**, 837-850.

Gray, W., 1968. Global view of the origin of tropical disturbances and tropical storms. *Mon. Wea. Rev.*, **96**, 669-700.

Heymsfield, G. M., J. B. Halverson, J. Simpson, L. Tian, P. Bui,2001 ER-2 Doppler Radar (EDOP) Investigations of the Eyewall of Hurricane Bonnie During CAMEX-3, *J. Appl. Meteor.*,, **40**, 1310-1330.

_____, J. B. Halverson, and I.J. Caylor, 1999: A wintertime gulf coast squall line observed by EDOP airborne Doppler radar. *Mon. Wea. Rev.*, **127**, 2928-2949.

_____, S. Bidwell, I. J. Caylor, S. Ameen, S. Nicholson, W. Boncyk, L. Miller, D. Vandemark, P. E. Racette, and L. R. Dod, 1996: The EDOP radar system on the high altitude NASA ER-2 aircraft. *J. Atmos. Oceanic Tech.*, **13**, 795-809.

HFP2001, 2001: 2001 Hurricane Field Program Plan. [Available from Hurricane Research Division, NOAA/Atlantic Oceanographic and Meteorological Laboratory, Miami, FL].

Hock, T. F., and J. L. Franklin, 1999: The NCAR GPS dropwindsonde. *Bull. Amer. Meteor. Soc.*, **80**, 407-420.

Holliday, C.R. and A.H. Thompson, 1979: Climatological characteristics of rapidly intensifying typhoons. *Mon. Wea. Rev.*, **107**, 1022-1034.

Hood et al., 2004: CAMEX (this issue).

Jones, S. C., 1995: The evolution of vortices in vertical shear. Part I: Initially barotropic vortices. *Quart. J. Roy. Meteor. Soc.*, **121**, 821-851.

Malkus, J. S. and H. Riehl, 1960: On the dynamics and energy transformations in steady state hurricanes, *Tellus*, **12**, 1-20

Marks, F.D., R.A. Houze, Jr. and J.F. Gamache, 1992: Dual-aircraft investigation of the inner core of Hurricane Norbert. Part I: Kinematic Structure. *J. Atmos. Sci.*, **49**:919-942.

May, R. D., 1998: Open-path, near-infrared tunable diode laser spectrometer for atmospheric measurements of H_20. *J. Geophys. Res.*, **103**, 19,161-19,172.

Montgomery, M. T., and J. Enagonio, 1998: Tropical cyclogenesis via convectively forced vortex Rossby waves in a three-dimensional quasi-geostrophic model. *J. Atmos. Sci.*, **55**, 3176-3207.

QuikSCAT, 2001: QuikSCAT science data product user's manual: Overview and geophysical data products. Version 2.2, Report number D-18053, 89 pp. [Available from Jet Propulsion Laboratory, Pasadena, CA]

Sadowy, G. A., A. C. Berkun, W. Chun, E. Im, and S. L. Durden, 2003: Development of an advanced airborne precipitation radar. *Microwave J.*, **46**, 84-98.

Simpson, R.H., Ed., 2002: Hurricane! Coping with disaster. *Amer., Geophys Un.*, Washington, D.C. 360 pp.

Simpson, J., J.B. Halverson, B. S. Ferrier, W. A. Petersen, R.H. Simpson, R. Blakeslee, and S. L. Durden, 1998: On the role of "hot towers" in tropical cyclone formation, *Meteorology and Atmos. Physics*, **67**, 15-35.

_____, E. Ritchie, G.J. Holland, J. Halverson, and S. Stewart, 1997. Mesoscale interactions in tropical cyclone genesis. *Mon. Wea. Rev.*, **125**, 2643-2661.

Steranka, J., E.B. Rodgers and R. C. Gentry, 1986: The relationship between satellite measured convective bursts and tropical cyclone intensification. *Mon. Wea. Rev.*, **114**, 1539-1546.

Wentz, F. J., C. Gentemann, D. Smith, D. Chelton, 2000: Satellite measurements of sea surface temperature through clouds. *SCIENCE*, **288**, 847-850.

Zehr, R. M., 1992: Tropical cyclogenesis in the western North Pacific. NOAA Tech. Rep. NESDIS 61, 181 pp. [Available from NOAA/NESDIS, E/RA22, 5200 Auth Road, Washington, DC 20233.]

_____, 2003: Environmental vertical wind shear with Hurricane Bertha (1996). *Mon. Wea. Rev.*, **126**, 345-356.

Figure Captions

Figure 1. Tropical Storm Chantal "best track". Minimum mean sea-level pressure (MSLP) in hPa, and maximum surface winds (MSW) in meters per second are shown at 3 h intervals.

Figure 2. Time history of Tropical Storm Chantal from 18 - 22 August. Panel A shows MSLP and MSW traces, Panel B shows storm advection speed and direction, and Panel C shows model-calculated vertical shear. See text for details.

Figure 3. Satellite images from GOES and TRMM on 20August 2001. Shown are panel A) GOES visible image at 2002 UTC, Panel B) GOES IR (10.8) μm image at 2002 UTC, and Panel C) TRMM TMI 85 GHz image at 2034 UTC. The edge of the TRMM swath is noted on the lower half of Panel C. The ER-2 and DC-8 flight tracks are superimposed on Panel B, and the NOAA-42 P3 flight track is shown on Panel C. ER-2 and DC-8 passes 1-3 are indicated on Panel B. Grid lines are in 1° intervals.

Figure 4. Large scale surface conditions. Panel A provides 3-day averaged SST's derived from TMI. Panel B shows surface winds derived from the QuikSCAT Level 2b product. Chantal's track is superimposed on both panels and 200 K (solid) and 240 K (dashed) IR brightness temperature contours are provided for reference.

Figure 5. Vertical environmental structure at 1200 UTC on 20 August 2001. Skew-T plots from MID, KCR, and KJP are shown in Panels A-C, respectively. Panel D shows the vertical u, v

wind profile, and 200 to 850 hPa shear vector derived from the NCEP "final analysis". Barbs: flag is 5 ms^{-1}, half-flag is 2.5 ms^{-1}, and pennant is 25 ms^{-1}.

Figure 6. IR images covering period of ER-2 flights on 20 August 2001. The color table highlights the cold over shooting cloud tops and the cirrus outflow from them. The two cells comprising the main convective burst and the expanding anvil are indicated by dashed lines. The center obtained from the storm "is indicated. The 2002 UTC panel shows the 200 hPa to 850 hPa shear vector obtained from the NCEP 20 August 2001 at 1200 UTC analysis (Fig. 5D). Grid lines are in 0.4° intervals.

Figure 7. Growth of Cell 2. Shown are: cloud top temperatures from cells 1-3 (Panel A) and IR cloud top area (Panel B). The area curves in Panel B are thresholded for 194 K, 196 K and 198 K. The times where the ER-2 passed across Cell 2 (vertical dashed lines) provide a time reference. The tropopause minimum sounding temperature (~192 K) is indicated in Panel A. See text for details.

Figure 8. Locations of dropsondes released from the DC-8 and NOAA-42 P3. The storm "best track" is superimposed and dropsondes used in Fig. 10 are indicated by (★).

Figure 9. Horizontal analyses based on flight-level data and dropsondes at A) 11.7 km, B) 4.3 km, and C) 0.2 km MSL. The background images in each panel are from GOES (Panel A) and TRMM (Panels B, C) satellite observations. All panels show θ_E contours at labeled values to highlight features. Wind barbs are given in panels A and B (pennant: is 25 ms^{-1}; flag: 5 ms^{-1}; half-flag: 2.5 ms^{-1}), and streamlines are shown in all panels. See text for details.

Figure 10. Skew-T and θ_E plots from dropsondes locations indicated in by (★) in Fig. 8. Dropsondes are all from the DC-8 except in Panel D where the 2101 UTC DC-8 drop is plotted with the 2058 UTC P3 drop in θ_E panel since there were no low level dew point measurements from the DC-8 dropsonde. Wind barbs: pennant: is 25 ms^{-1}; flag: 5 ms^{-1}; half-flag: 2.5 ms^{-1}.

Figure 11. Horizontal analyses of temperature perturbation (Panels A, B, C, D) at 50 m (SFC), 4, 6, and 8 km altitude and pressure perturbation (Panels E, F) at SFC and 4 km altitude based on dropsonde data. The approximate location of Cell 2 (gray-shaded circular region), the LLC, and low ("L") and high ("H") pressure centers are indicated on each panel. Contours are given in 1°C and 1 hPa intervals except where noted; negative contours are dashed. Local minima and maxima are shown in italics.

Figure 12. Cross section obtained from ER-2 Doppler Radar (EDOP) for Pass 2 between 2101-2125 UTC. Panel A is a color-enhanced reflectivity image with superimposed storm relative wind vectors obtained from EDOP, contours of θ_E (black). Panel B is a color-enhanced image of along-track winds (u_r) with superimposed contours of the transverse (v_r) wind component (black), and approximate streamlines (white). The contours are based on the DC-8 and P3 flight level and dropsonde data; they terminate in the convective region where data is too sparse to draw contours. Positive v_r is into the page and the vortex maximum winds are noted by solid dot (into page) and "+" (out of page). The orientation of the section is shown in Fig. 3. Reflectivities (w) exceeding 50 dBZ (8 ms^{-1}) are white, and w less than -8 ms^{-1} are black. Locations of

dropsonde start times are in italics and dropsonde and flight-level data are shown by small numbers.

Figure 13. Similar to Fig. 6 except for Pass 3 at 2148-2224 UTC flight line.

Figure 14. Conceptual summary of Tropical Storm Chantal derived from aircraft and satellite observations.

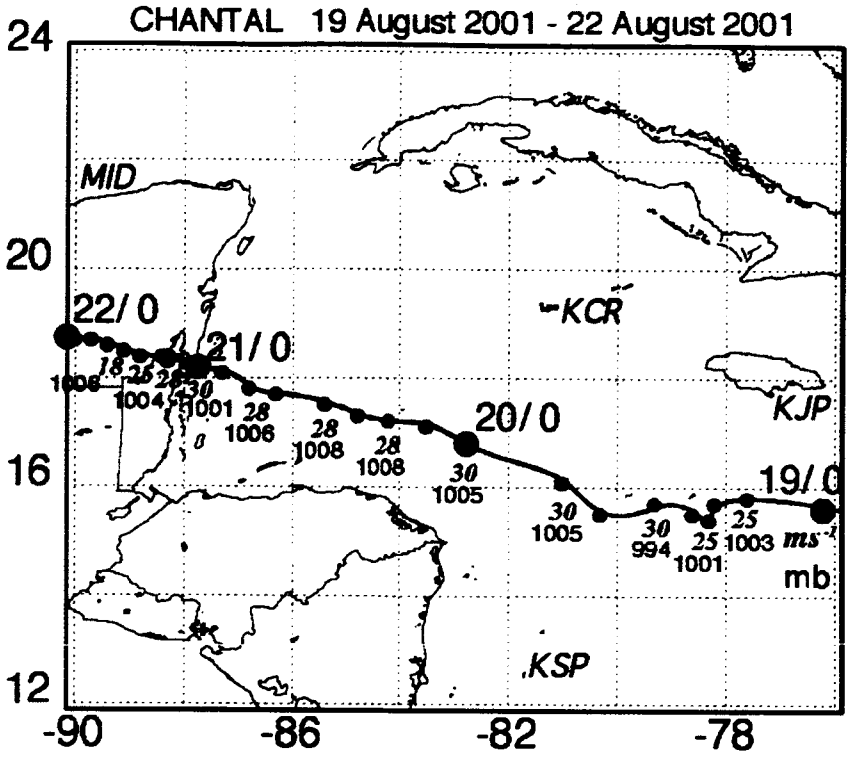

Figure 1. Tropical Storm Chantal "best track". Minimum mean sea-level pressure (MSLP) in hPa, and maximum surface winds (MSW) in meters per second are shown at 3 h intervals.

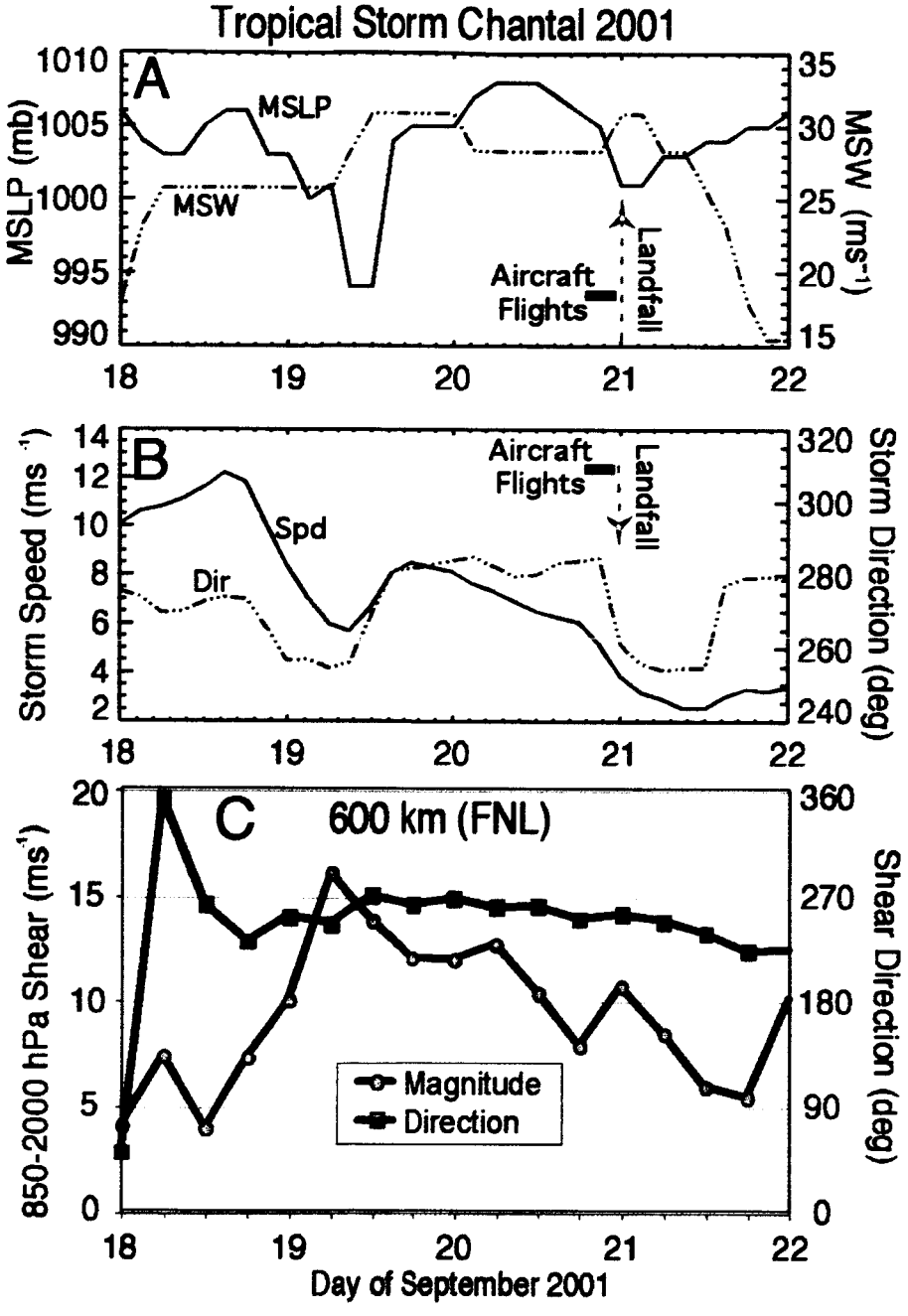

Figure 2. Time history of Tropical Storm Chantal from 18 - 22 August. Panel A shows MSLP and MSW traces, Panel B shows storm advection speed and direction, and Panel C shows model-calculated vertical shear. See text for details.

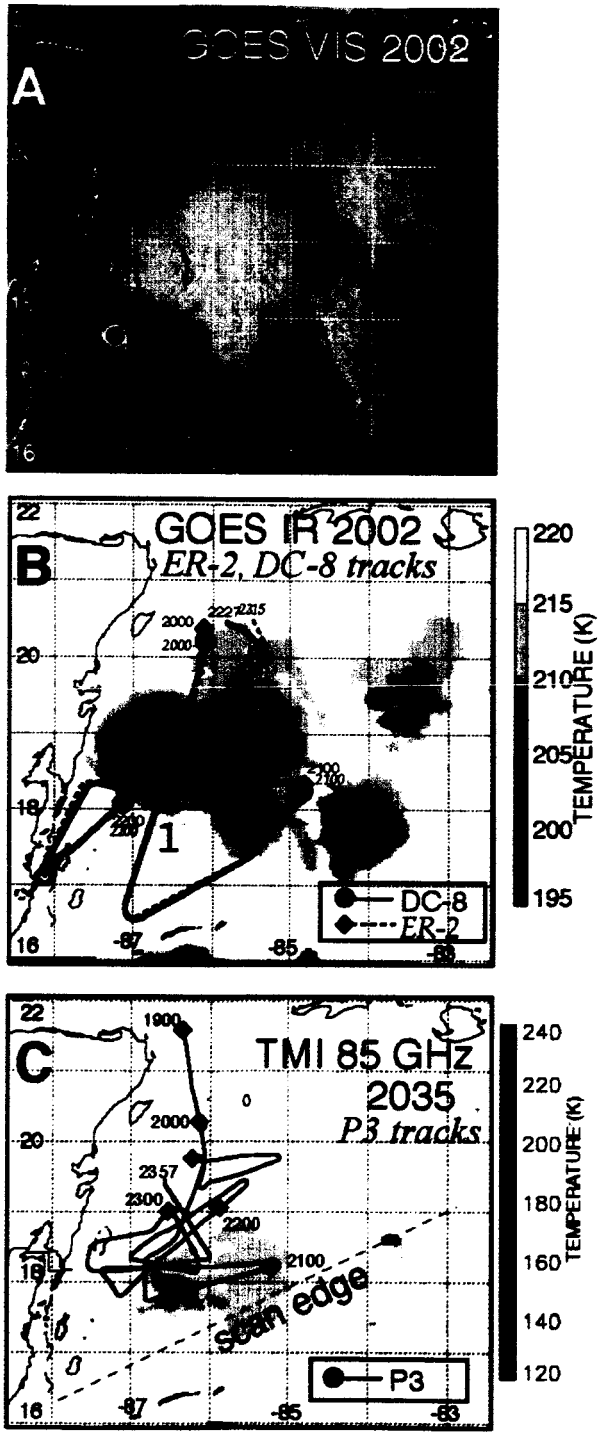

Figure 3. Satellite images from GOES and TRMM on 20August 2001. Shown are panel A) GOES visible image at 2002 UTC, Panel B) GOES IR (10.8) μm image at 2002 UTC, and Panel C) TRMM TMI 85 GHz image at 2034 UTC. The edge of the TRMM swath is noted on the lower half of Panel C. The ER-2 and DC-8 flight tracks are superimposed on Panel B, and the NOAA-42 P3 flight track is shown on Panel C. ER-2 and DC-8 passes 1-3 are indicated on Panel B. Grid lines are in 1° intervals.

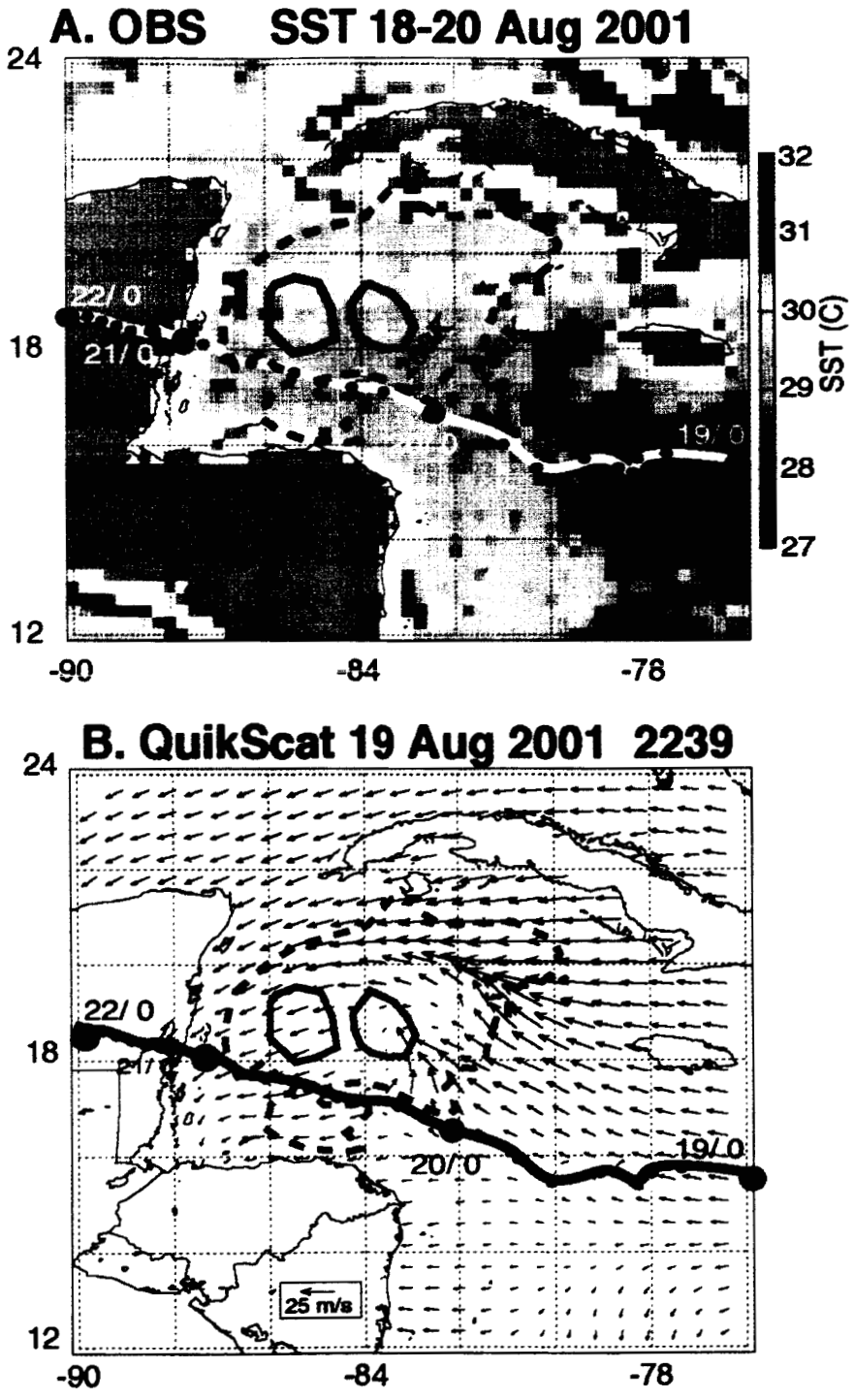

Figure 4. Large scale surface conditions. Panel A provides 3-day averaged SST's derived from TMI. Panel B shows surface winds derived from the QuikSCAT Level 2b product. Chantal's track is superimposed on both panels and 200 K (solid) and 240 K (dashed) IR brightness temperature contours are provided for reference.

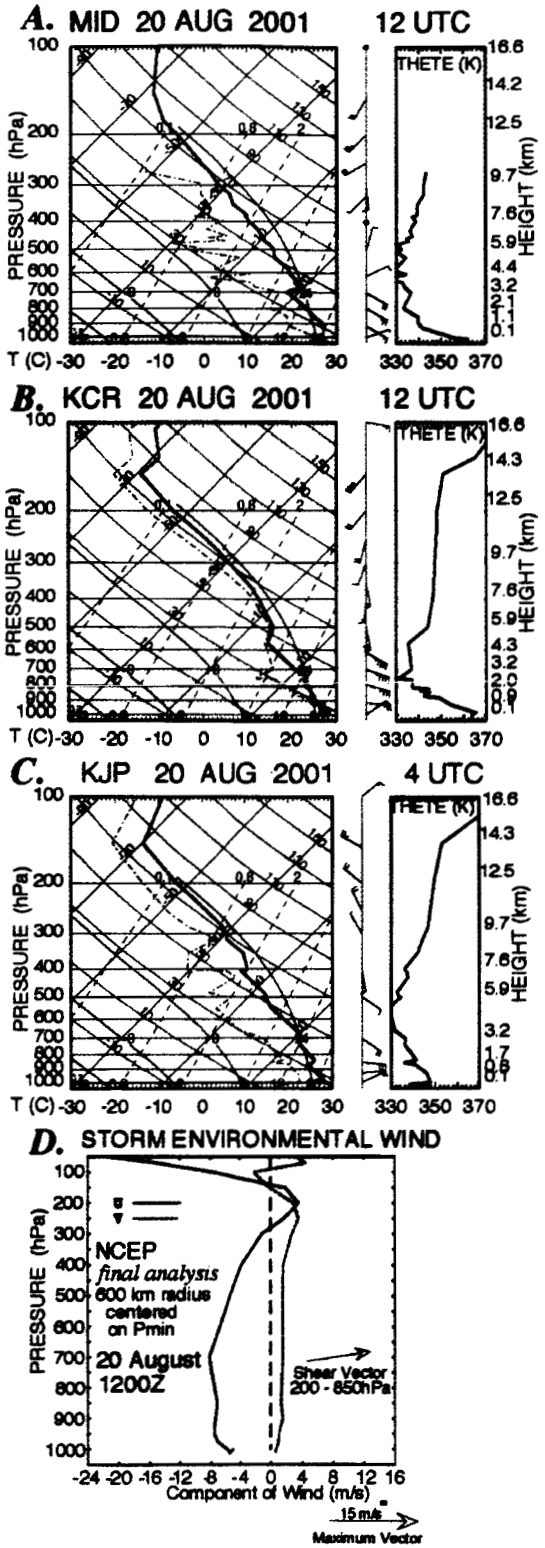

Figure 5. Vertical environmental structure at 1200 UTC on 20 August 2001. Skew-T plots from MID, KCR, and KJP are shown in Panels A-C, respectively. Panel D shows the vertical u, v wind profile, and 200 to 850 hPa shear vector derived from the NCEP "final analysis". Barbs: flag is 5 ms^{-1}, half-flag is 2.5 ms^{-1}, and pennant is 25 ms^{-1}.

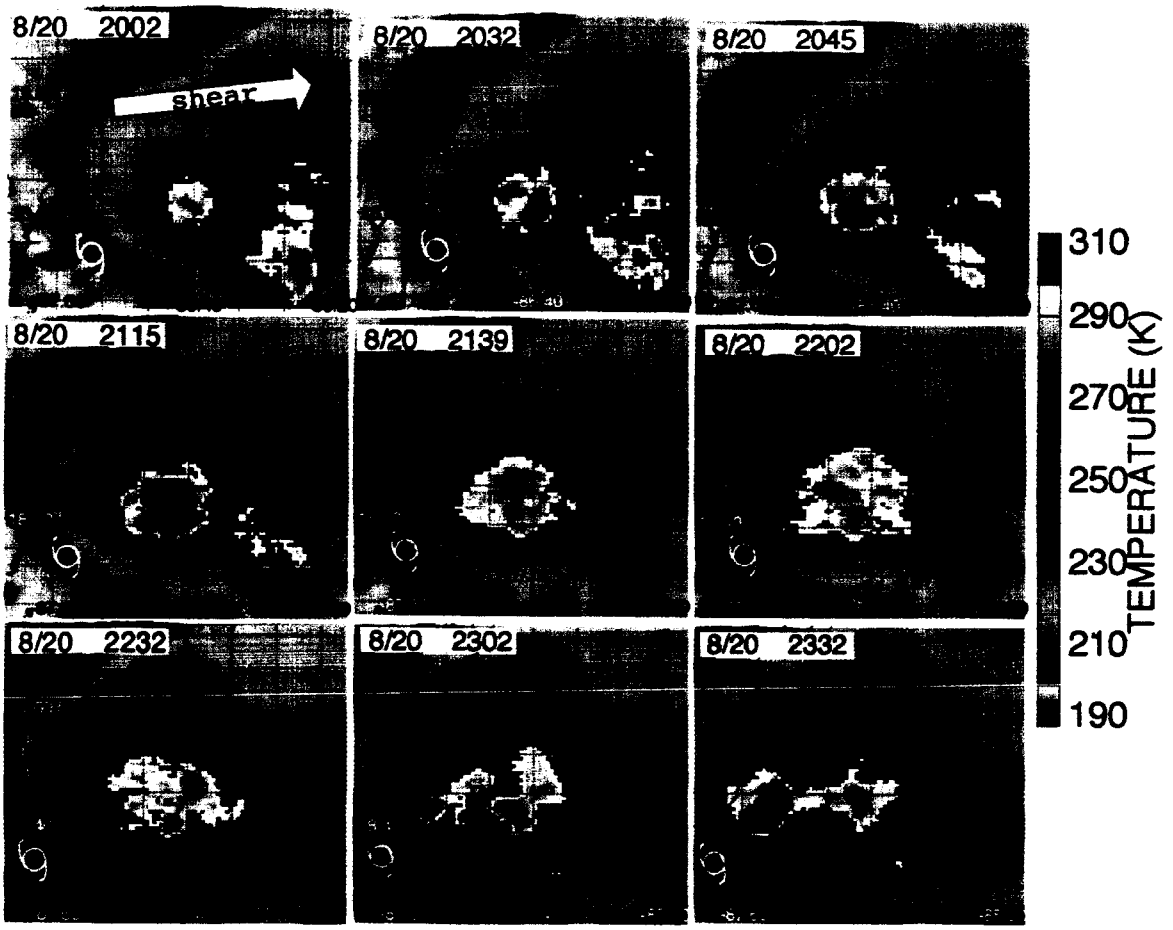

Figure 6. IR images covering period of ER-2 flights on 20 August 2001. The color table highlights the cold over shooting cloud tops and the cirrus outflow from them. The two cells comprising the main convective burst and the expanding anvil are indicated by dashed lines. The center obtained from the storm "is indicated. The 2002 UTC panel shows the 200 hPa to 850 hPa shear vector obtained from the NCEP 20 August 2001 at 1200 UTC analysis (Fig. 5D). Grid lines are in 0.4° intervals.

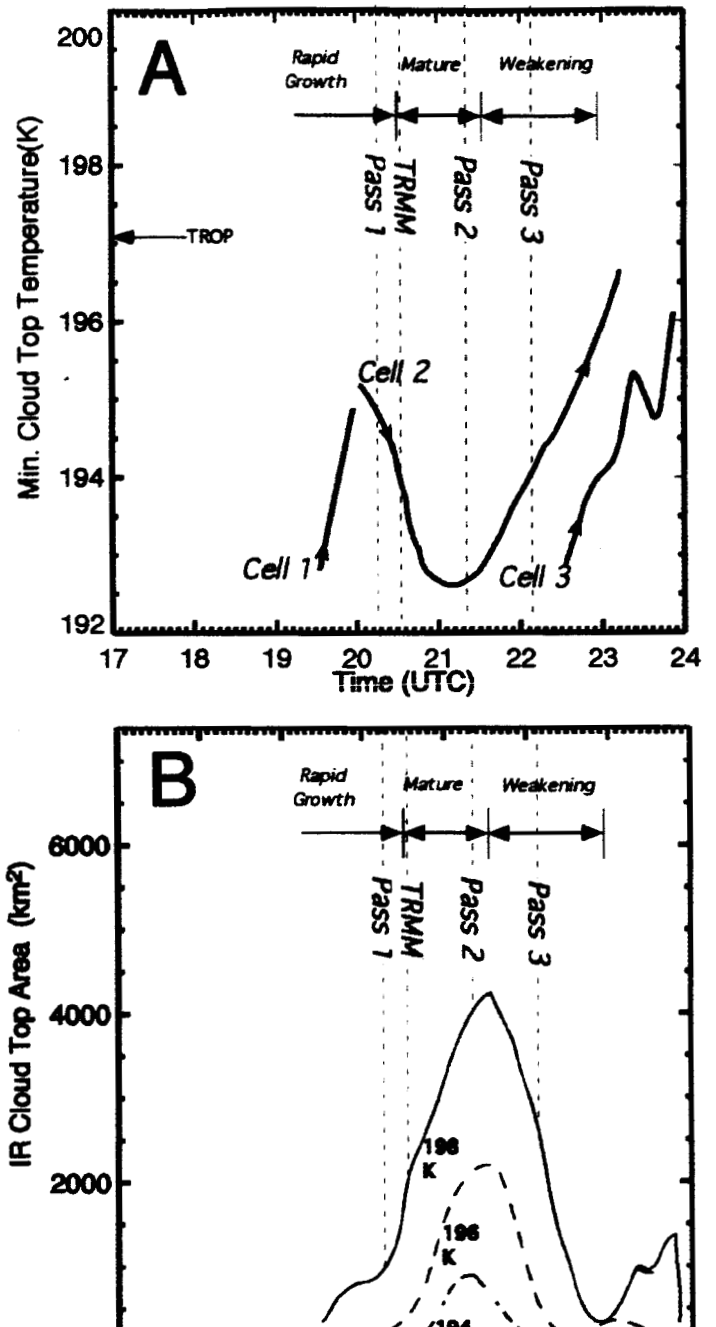

Figure 7. Growth of Cell 2. Shown are: cloud top temperatures from cells 1-3 (Panel A) and IR cloud top area (Panel B). The area curves in Panel B are thresholded for 194 K, 196 K and 198 K. The times where the ER-2 passed across Cell 2 (vertical dashed lines) provide a time reference. The tropopause minimum sounding temperature (~192 K) is indicated in Panel A. See text for details.

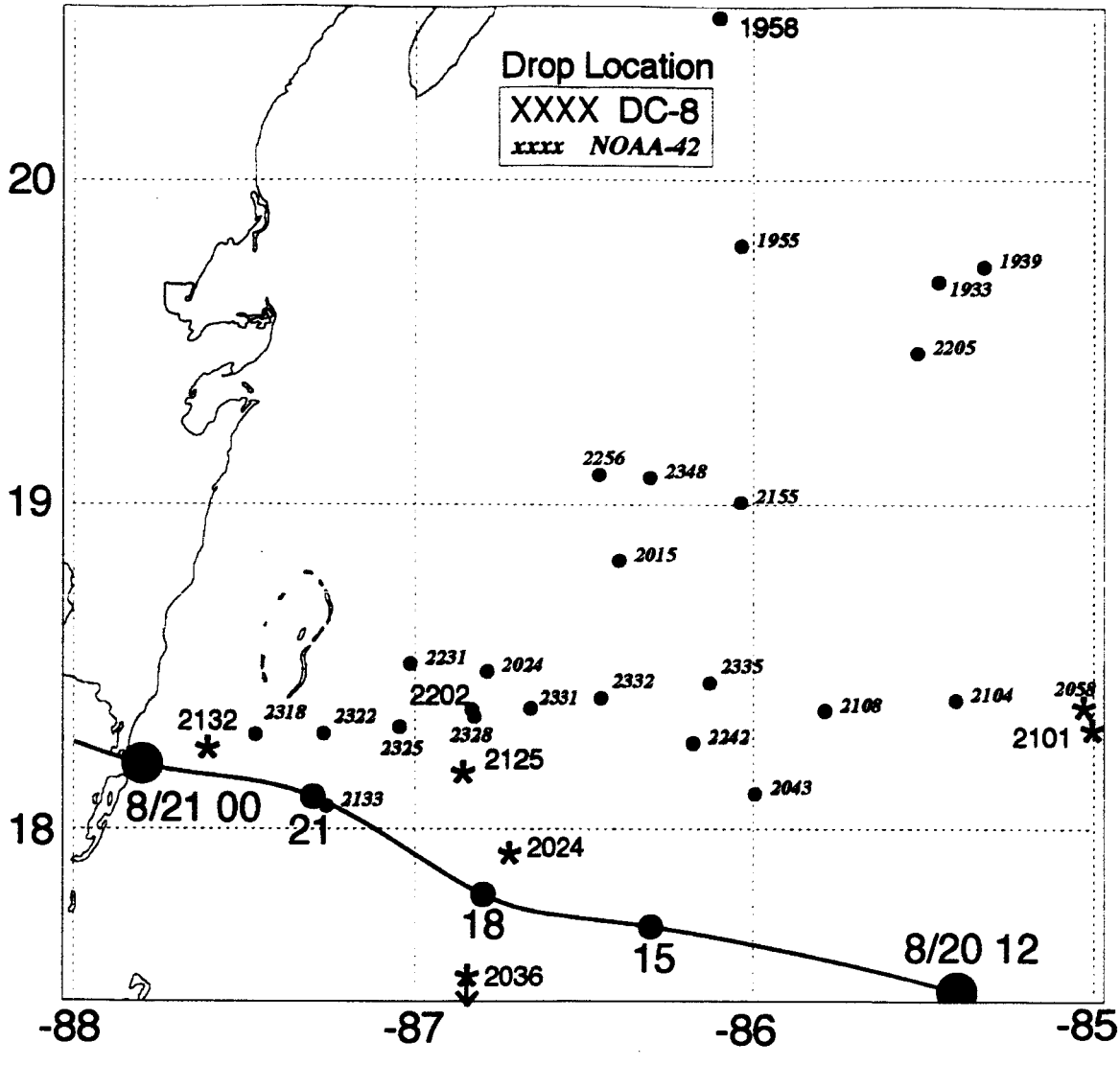

Figure 8. Locations of dropsondes released from the DC-8 and NOAA-42 P3. The storm "best track" is superimposed and dropsondes used in Fig. 10 are indicated by (★).